Inorganic carbon in the Indian Ocean: Distribution and dissolution processes

Christopher L. Sabine
Joint Institute for the Study of Atmosphere and Ocean, University of Washington, Seattle, Washington, USA

Robert M. Key
Atmospheric and Oceanic Sciences Program, Princeton University, Princeton, New Jersey, USA

Richard A. Feely and Dana Greeley
NOAA/Pacific Marine Environmental Laboratory, Seattle, Washington, USA

Received 15 January 2002; revised 14 May 2002; accepted 14 June 2002; published 24 October 2002.

[1] This study uses nearly 25,000 carbon measurements from the WOCE/JGOFS global CO_2 survey to examine the distribution of dissolved inorganic carbon (DIC) and total alkalinity (TA) in the Indian Ocean. Shallow and intermediate distributions of inorganic carbon do not strictly follow temperature and salinity because of differing surface gradients and vertical biological processes that work to modify the circulation derived features. Anthropogenic CO_2 has increased the shallow DIC by as much as 3%, decreasing the vertical DIC gradient. Deep ocean DIC and TA increase toward the north because of the decomposition and dissolution of organic and inorganic particles. Calcite saturation depths range from 2900–3900 m with the deepest saturation depth in the central Indian Ocean. Variations of aragonite saturation depth (200–1400 m) are similar to calcite, but the deepest saturations are in the southwestern Indian Ocean. The shallowest aragonite saturation depths are found in the Bay of Bengal. In the northern Arabian Sea and Bay of Bengal, the current aragonite saturations are 100 and 200 m shallower, respectively, than in preindustrial times. Estimates of carbonate dissolution rates on isopycnal surfaces range from 0.017 to 0.083 μmol kg^{-1} yr^{-1} in deep waters. Upper water column dissolution rates range from 0 to 0.73 μmol kg^{-1} yr^{-1}, with a local maximum occurring in intermediate waters just below the aragonite saturation horizon. Dissolution is also generally higher north of the Chemical Front at 10–20°S. There is some evidence for significant sedimentary sources in the northern Indian Ocean. *INDEX TERMS:* 9340 Information Related to Geographic Region: Indian Ocean; 4805 Oceanography: Biological and Chemical: Biogeochemical cycles (1615); 4806 Oceanography: Biological and Chemical: Carbon cycling; 4825 Oceanography: Biological and Chemical: Geochemistry; *KEYWORDS:* Indian Ocean, carbon cycle, alkalinity, calcium carbonate, total CO_2, saturation state

Citation: Sabine, C. L., R. M. Key, R. A. Feely, and D. Greeley, Inorganic carbon in the Indian Ocean: Distribution and dissolution processes, *Global Biogeochem. Cycles*, *16*(4), 1067, doi:10.1029/2002GB001869, 2002.

1. Introduction

[2] As concerns grow over the fate of anthropogenic CO_2 in the oceans, it becomes increasingly important to understand the fundamental processes controlling the current distributions of dissolved inorganic carbon (DIC) and total alkalinity (TA) in the oceans. In the mid 1990s, several carbon measurement programs focused on the Indian Ocean, greatly increasing the existing carbon database for this basin. The morphology of the Indian Ocean, with a northern boundary in the tropics, generates a circulation system that is unique to this ocean [*Wyrtki*, 1973]. Features like the seasonally changing monsoon gyre, the exceptionally strong southern hemisphere western boundary current and lack of well developed eastern boundary current, and the hydrochemical front at about 10–20°S have a direct impact on the Indian Ocean carbon cycle.

[3] This work focuses on the distributions of two carbon species that are controlled by differing processes. DIC is strongly influenced by the biological pump [e.g., *Redfield et al.*, 1963; *Volk and Hoffert*, 1985]. Phytoplankton production at the surface removes carbon from the surface waters. As the phytoplankton die and sink through the water column, the particulate organic carbon is remineralized to DIC at depth. DIC is also influenced by gas exchange as

0886-6236/02/2002GB001869$12.00

part of the solubility pump. The uptake of anthropogenic CO_2 is directly reflected as an increase in DIC concentrations [e.g., *Brewer*, 1978; *Chen and Millero*, 1979]. TA is not affected by gas exchange. The physical uptake of anthropogenic CO_2 does not change the TA concentration of the waters. TA is also relatively insensitive to organic carbon production/remineralization. TA is altered by the uptake/release of protons associated with reduction/oxidation of some nutrients [e.g., *Brewer et al.*, 1975; *Brewer and Goldman*, 1976; *Chen et al.*, 1982], but this effect is small. TA distributions in the ocean are primarily controlled by circulation and the production/dissolution of calcium carbonate. In the open ocean, the production of carbonate tests by marine phytoplankton (e.g., coccoliths) and zooplankton (e.g., forams, pteropods) decreases the TA of surface waters. As these particles sink out of the surface ocean they begin to dissolve. For many years, this dissolution was thought to occur only at great depths, below the ''carbonate lysocline'' [*Sverdrup et al.*, 1941; *Bramlette*, 1961; *Broecker and Takahashi*, 1977]. The dissolution of carbonate particles in shallow sediments has been known for many years, but has not been widely recognized as significant to the global carbonate budget [e.g., *Aller*, 1982]. Recent evidence, however, has suggested that the majority of the open ocean carbonate exported from the surface layer is remineralized in the upper 500–1000 m, well above the calcite lysocline [*Milliman et al.*, 1999]. The observed carbon distributions provide insight into carbonate remineralization in the Indian Ocean.

[4] The relationship between DIC and TA defines the inorganic carbon system of the oceans. With a proper knowledge of the carbonate dissociation constants one can use DIC and TA to accurately calculate the concentrations of all the carbonate species. The DIC/TA ratio influences the ocean's capacity to take up anthropogenic CO_2 by determining the buffer capacity. It has also been shown that the DIC/TA ratio influences the effect of temperature changes on pCO_2 [*Copin-Montegut*, 1988, 1989; *Goyet et al.*, 1993], and helps determine how corrosive waters are to carbonate particles. In this paper, we use the WOCE/JGOFS global CO_2 survey data from the Indian Ocean to examine the distribution of DIC and TA in the Indian Ocean. This study provides a benchmark of carbon distributions against which future CO_2 survey cruises can be compared. We also provide new estimates of calcium carbonate dissolution rates in the water column based upon changes in TA.

2. Data and Methods

[5] The majority of the samples used for this study were collected as part of the U.S. WOCE/JGOFS Indian Ocean survey (December 1994–January 1996). These data were strengthened and extended with the French INDIGO I (February–March 1985), II (April 1986), and III (January–February 1987) and CIVA-1 (February–March 1993; WOCE designation I6S) cruises [*Poisson et al.*, 1988, 1989, 1990] and the U.S. WOCE S4I section (May–July 1996). The combined data set includes 1512 stations. After WOCE quality control procedures [*Corry et al.*, 1994] the data set is composed of approximately 24,600 DIC and 22,900 TA measurements. TA was determined by closed cell titration as summarized by *Millero et al.* [1998b]. DIC was determined by coulometry [*Johnson et al.*, 1985, 1998]. Certified Reference Materials [*Dickson*, 1990; *Dickson et al.*, 2002a, 2002b] were used to validate the instrument calibrations for both parameters. The data set used here is the same as that used by *Sabine et al.* [1999] to examine the distribution of anthropogenic CO_2 in the Indian Ocean except that no GEOSECS results were included. The station locations are shown in Figure 1.

2.1. Data Quality

[6] Once the data set was compiled, a crossover analysis was carried out to determine whether significant systematic offsets existed between the various cruises. R. M. Key (WOCE Indian Ocean survey: Data comparison at crossover stations, available at http://geoweb.princeton.edu/people/resstaff/key/key.cross/crossover.html) devised and carried out the procedure for the WOCE/JGOFS Indian Ocean survey cruises. These results were presented by *Millero et al.* [1998b] for the alkalinity measurements and by *Johnson et al.* [1998] for the DIC measurements. Sabine extended this procedure to include the French cruises and WOCE S4I [*Sabine et al.*, 1999]. For the U.S. WOCE sections, including S4I, the mean leg to leg differences for DIC (1.8 ± 0.8 μmol kg^{-1}) and TA (2.4 ± 1.6 μmol kg^{-1}) were approximately the same as the error estimated from duplicate and CRM analyses: ~2 μmol kg^{-1} for DIC [*Johnson et al.*, 1998] and 4 μmol kg^{-1} for TA [*Millero et al.*, 1998b]. The crossover analysis demonstrated that the CIVA-1 results were equivalent to U.S. results in precision and accuracy. The INDIGO results, which were measured before the availability of CRMs, were systematically offset from the WOCE results and were adjusted as described by *Sabine et al.* [1999]. After adjusting the INDIGO data, the entire data set is internally consistent to ±2.2 and 3.0 μmol kg^{-1} for DIC and TA, respectively.

2.2. Constants and Equations

[7] Wherever thermodynamic calculations were necessary we have used the carbonate equilibrium constants of *Mehrbach et al.* [1973] as refit by *Dickson and Millero* [1987]. A detailed examination of the potential result of this choice is given by *Millero* [1995]. The source for other equilibrium constants is summarized in Table 1, which adopts the symbolism used by *Department of Energy* (DOE) [1994, chap. 2, Table 1]. The concentrations of borate, sulfate, calcium, and fluoride were estimated using the equations of *Uppström* [1974], *Morris and Riley* [1966], *Millero* [1982], and *Riley* [1965], respectively. The constants were adjusted to pressures other than one atmosphere using the equations of *Millero* [1983]. All calculations were made using a general purpose FORTRAN code with the corrections noted by *Lewis and Wallace* [1998]. Our code was checked for consistency with that of *Lewis and Wallace* [1998] and also *DOE* [1994] as implemented by A. Dickson.

[8] Anthropogenic CO_2 estimates for the Indian Ocean are based on the ΔC* approach as discussed by *Sabine et al.* [1999]. The basic concept of the calculation can be expressed in terms of the following equation:

$$C_{anth}\left(\frac{\mu mol}{kg}\right) = C_m - \Delta C_{bio} - \Delta C_{eq280} - \Delta C_{diseq}, \qquad (1)$$

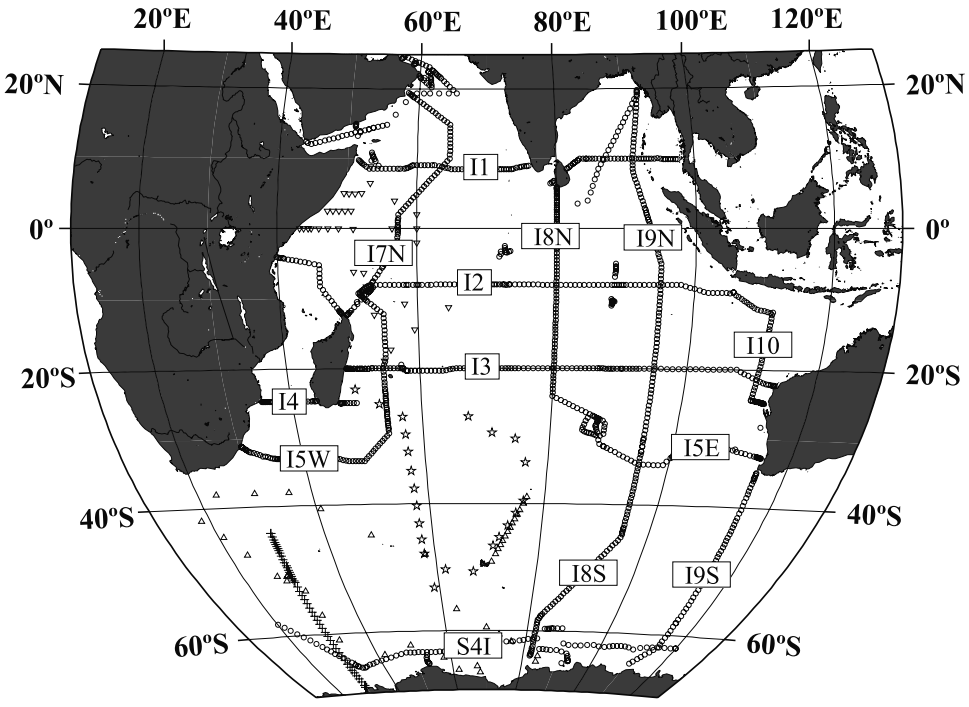

Figure 1. Station locations used for WOCE Indian Ocean (circles), CIVA 1/I6 (crosses), INDIGO I (stars), INDIGO II (inverted triangles), and INDIGO III (triangles) survey cruises.

where

C_{anth} = anthropogenic carbon concentration;
C_m = measured DIC concentration in μmol kg^{-1};
ΔC_{bio} = DIC (μmol kg^{-1}) changes resulting from the remineralization of organic matter and dissolution of calcium carbonate particles;
C_{eq280} = DIC (μmol kg^{-1}) of waters in equilibrium with an atmospheric CO_2 concentration of 280 μatm;
ΔC_{diseq} = air-sea CO_2 difference (i.e., ΔpCO_2) expressed in μmol kg^{-1} of DIC.

The preindustrial DIC distributions discussed here were derived by subtracting the anthropogenic CO_2 estimates of *Sabine et al.* [1999] from the measured DIC concentrations.

[9] The carbonate dissolution estimates are based on techniques fully described by *Feely et al.* [2002]. The approach is similar to the ΔC* calculations in that the amount of calcium carbonate dissolved can be estimated from changes in TA after subtracting out the preformed alkalinity concentrations and the changes due to organic matter production/remineralization. Although this general approach has been used for years [e.g., *Brewer et al.*, 1975; *Chen et al.*, 1982], *Feely et al.* [2002] quantify this process by defining the TA* tracer,

$$TA^*\left(\frac{\mu mol}{kg}\right) = 0.5(NTA - NTA^\circ) + 0.0593AOU, \quad (2)$$

where AOU is the apparent oxygen utilization, NTA is the salinity normalized TA measurement (TA $\frac{35}{S}$) and NTA° is a salinity normalized preformed alkalinity based on the equation of *Sabine et al.* [1999],

$$TA^\circ\left(\frac{\mu mol}{kg}\right) = 378.1 + 55.22S + 0.0716PO - 1.236\theta. \quad (3)$$

Table 1. Equilibrium Constants

Constant	Chemistry	Reference[a]
K_0	$[CO_2^*]/f(CO)_2$	*Weiss* [1974]
K_1	$[H^+][HCO_3^-]/[CO_2^*]$	*Dickson and Millero* [1987] *Mehrbach et al.* [1973]
K_2	$[H^+][CO_3^{-2}]/[HCO_3^-]$	*Dickson and Millero* [1987] *Mehrbach et al.* [1973]
K_W	$[H^+][OH^-]$	*Millero* [1995]
K_B	$[H^+][B(OH)_4^-]/[B(OH)_3]$	*Dickson* [1990] *Millero* [1995]
K_S	$[H^+]_F[SO_4^-]/[HSO_4^-]$	*Khoo et al.* [1977][b]
K_F	$[H^+][F^-]/[HF]$	*Dickson and Riley* [1979][c]
K_{1P}	$[H^+][H_2PO_4^-]/[H_3PO_4]$	*Yao and Millero* [1995] *Millero* [1995]
K_{2P}	$[H^+][HPO_4^{-2}]/[H_2PO_4^-]$	*Yao and Millero* [1995] *Millero* [1995]
K_{3P}	$[H^+][PO_4^{-3}]/[HPO_4^{-2}]$	*Yao and Millero* [1995] *Millero* [1995]
K_{Si}	$[H^+][SiO(OH)_3^-]/[Si(OH)_4]$	*Yao and Millero* [1995] *Millero* [1995]
$K_{calcite}$	$[Ca^{+2}][CO_3^{-2}]/[CaCO_3]$	*Mucci* [1983]
$K_{aragonite}$	$[Ca^{+2}][CO_3^{-2}]/[CaCO_3]$	*Mucci* [1983]

[a] A number of typographical errors have been found in these papers. *Lewis and Wallace* [1998] have published a listing of these errors in addition to a program to make various carbonate system calculations.
[b] Free hydrogen ion scale. See also *Millero* [1995] and references therein.
[c] pH scale changed to total.

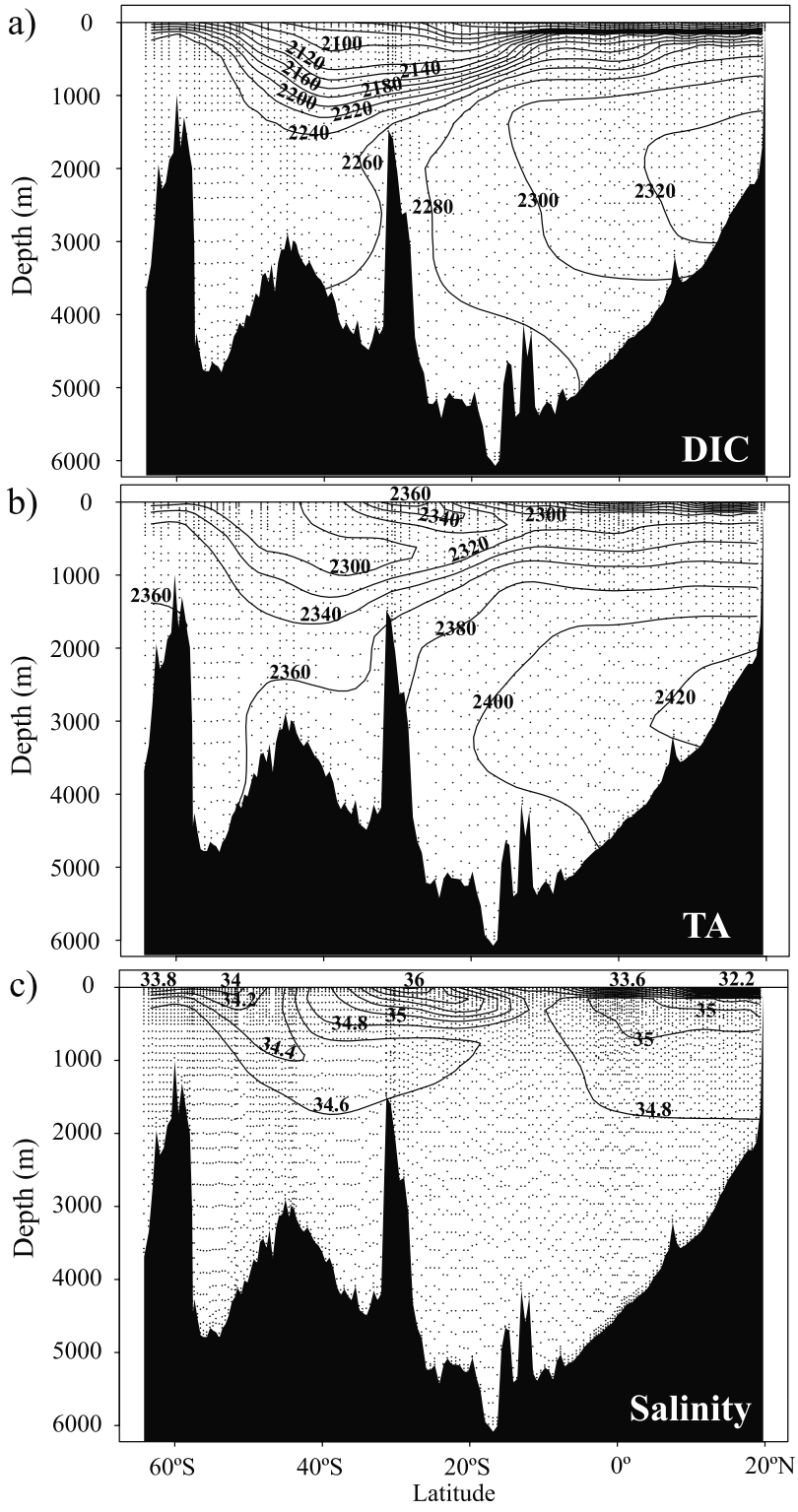

Figure 2. Sections of (a) DIC, (b) TA, and (c) Salinity along I9°N and I8°S in the eastern Indian Ocean (∼93°E). Points indicate sample locations.

S is salinity, θ is potential temperature, and PO = O_2 + 170 HPO_4^{-2}, taken from *Broecker* [1974]. The excess alkalinity is evaluated on isopycnal surfaces relative to a water mass age tracer (i.e., CFC age or ^{14}C age) to derive an average dissolution rate for that surface. The assumptions and shortcomings of this approach are discussed below and by *Feely et al.* [2002].

3. Carbon Distributions

[10] The distribution of carbon species in the water column determines the ocean's buffer capacity and the ability of the ocean to take up CO_2 from the atmosphere. Carbonate equilibrium in the ocean maintains an inverse relationship between pCO_2 and the pH of seawater. The oceanic uptake of anthropogenic CO_2 increases the DIC/TA ratio, and lowers the pH and buffer capacity of the waters. The dissolution of calcium carbonate in the water column counteracts this effect by decreasing the DIC/TA ratio, increasing the pH, and lowering pCO_2. Thus, in the long term, the amount and location of calcium carbonate dissolution can influence atmospheric CO_2 concentrations. *Archer and Maier-Reimer* [1994], for example, found that their model could not reproduce the magnitude of the glacial-interglacial atmospheric CO_2 variations without dissolution of carbonate particles above the calcite lysocline. This dissolution was assumed to be driven by organic remineralization in the sediments which resulted in higher glacial whole-ocean alkalinity values. The work presented here examines evidence of open ocean carbonate dissolution above the calcite lysocline. But first, the distributions of DIC, TA, and the DIC/TA ratio are examined to provide a better understanding of the Indian Ocean carbon chemistry.

3.1. Shallow and Intermediate Waters

[11] Figure 2 shows the meridional distribution of carbon and salinity in the eastern Indian Ocean. The distribution of DIC and TA in the thermocline waters of the South Indian Ocean reflect the characteristics of the subtropical gyre thermocline bowl with a downwarping of isolines at 40° to 50°S [*Wyrtki*, 1973]. This structure is not observed in the northern Indian Ocean. The low salinity Antarctic Intermediate Water (AAIW) is easily seen at the southern end of the salinity section [*Wyrtki*, 1973; *Fine*, 1993]. The TA section also shows a local minimum in this region; although this minimum is somewhat shallower and proportionally smaller than salinity. The difference derives from the surface TA distribution in the Southern Ocean. Over most of the tropical and subtropical oceans, surface TA values vary proportionally with salinity [*Millero et al.*, 1998a]. South of the Subtropical Convergence Zone, however, the TA to salinity ratio is much higher (see Southern Ocean designator in Figure 3). This presumably results from the upwelling of deep waters around Antarctica that have accumulated alkalinity from carbonate dissolution. This results in a much smaller meridional gradient in surface TA than salinity, and thus a smaller and displaced TA signal in the ocean interior. The TA minimum is much more pronounced in the eastern Indian Ocean than in the west. The northward and eastward displacement of the TA minimum suggests that this feature is more closely related to the Subantarctic Mode Water (SAMW) that is strongest in the eastern Indian Ocean as opposed to the AAIW that has its strongest component in the western and central Indian [*Fine*, 1993].

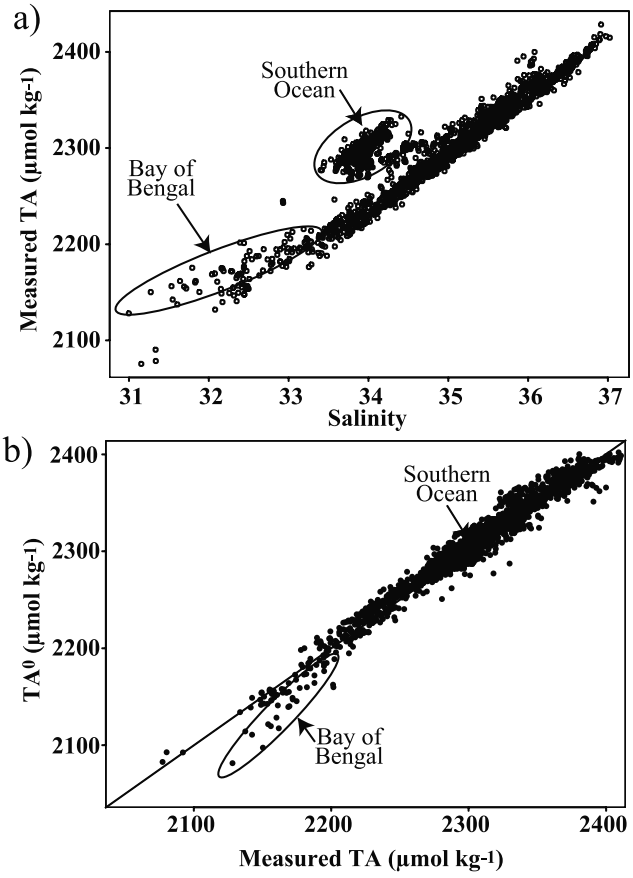

Figure 3. Plots of (a) measured TA versus salinity and (b) TA^0 versus measured TA for all Indian Ocean data shallower than 60 m.

[12] Neither the AAIW nor the SAMW are manifested as a minimum in DIC (Figure 2a). In fact, Antarctic surface waters have higher DIC concentrations than the subtropical and tropical Indian Ocean surface waters. More importantly, DIC in the ocean is strongly affected by biology and gas exchange. The observed DIC distribution resembles apparent oxygen utilization (AOU) more than salinity. DIC also does not reflect the alkalinity and salinity maximum in the subtropical surface waters (~30°S, Figure 2). In this case, the alkalinity signal is proportional to salinity and is likely caused by the same physical processes (i.e., excess evaporation).

[13] The third major feature observed in the shallow and intermediate waters is the strong surface minimum in all three parameters at the northern end of this section. This common feature results from fresh water dilution by rivers, such as the Ganges, that empty into the Bay of Bengal [*Rao et al.*, 1994]. The river influx, however, also brings in TA as indicated by the increase in TA relative to salinity in the Bay of Bengal surface waters (Figure 3a). The TA° equation determined by *Sabine et al.* [1999] accounts for the high Southern Ocean alkalinity values, but does not correct for

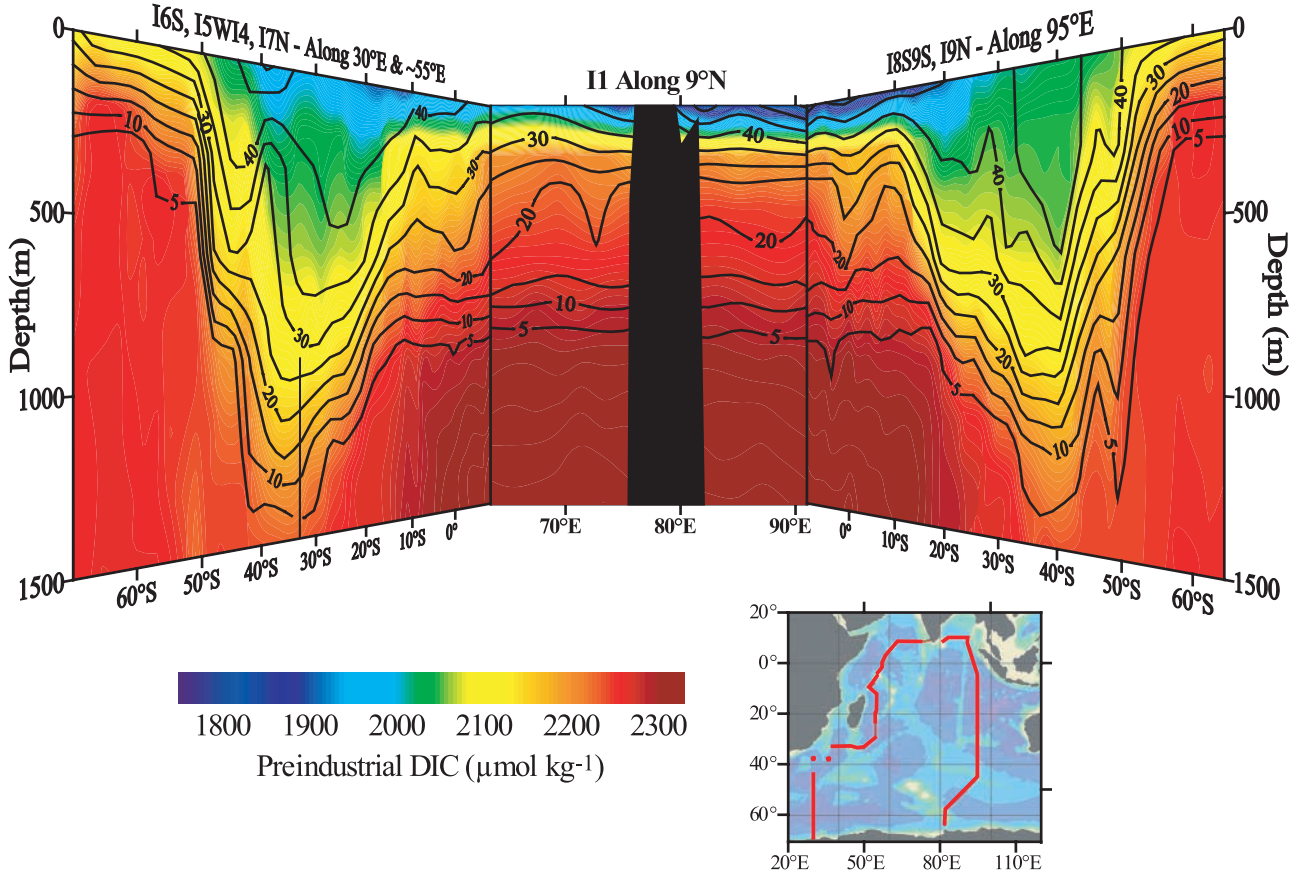

Figure 4. A 3-D image of preindustrial CO_2 (colors) and anthropogenic CO_2 (contours) along (from left to right) I6S, I5WI4, I7N, I1, I9N, and I8S.

the TA introduced by rivers (Figure 3b). This issue is discussed further in section 4.2.

[14] Observed DIC concentrations in the surface and intermediate waters of the Indian Ocean are contaminated with anthropogenic CO_2. *Sabine et al.* [1999] estimated the anthropogenic CO_2 concentrations for these same data using the ΔC^* approach. An estimate of the preindustrial DIC concentrations can be derived by subtracting the anthropogenic CO_2 estimates from the measured concentrations (Figure 4). Anthropogenic CO_2 is generally restricted to the waters with preindustrial concentrations less than 2250 μmol kg^{-1}. At the northern end of the Indian Ocean, where residence times are long and older waters are closer to the surface, the anthropogenic signal has penetrated into waters with higher preindustrial DIC concentrations. The highest anthropogenic CO_2 concentrations are observed at the surface in the Bay of Bengal and in the southern subtropical gyre where residence times at the surface are longest. Anthropogenic CO_2 has increased the observed DIC by up to 3% and is serving to decrease the vertical DIC gradient.

3.2. Deep Waters

[15] Thus far, anthropogenic CO_2 has not contaminated waters deeper than about 1500 m. In the deep Indian Ocean, there is little or no salinity gradient. Salinity increases by less than 0.05 between 60°S and 20°N in the eastern deep waters. DIC and TA, however, have significant increases toward the north because of the decomposition and dissolution of organic and inorganic particles falling into the deep ocean (Figure 2). As *Rubin and Key* [2002] noted, potential alkalinity (PALK = (TA + nitrate) $\frac{35}{S}$) has a strong linear correlation with natural ^{14}C in deep waters. Thus, PALK can be used in a manner similar to natural ^{14}C to infer deep ocean circulation. Figure 5 shows the distribution of PALK in the near bottom waters (within 50 m) of the Indian Ocean. The lowest values near the southeast coast of Africa correspond to deep waters (primarily North Atlantic Deep Water (NADW)) advected from the midlatitude South Atlantic [*Toole and Warren*, 1993]. These deep waters are warmer, saltier, higher in oxygen, and lower in TA and DIC than the Circumpolar Deep Water (CDW) south of 50°S. The CDW PALK values are relatively low compared to the older waters in the northern Indian Ocean that have had time to accumulate alkalinity from the dissolution of carbonate particles. The low PALK waters of the CDW move north in the eastern and western Indian Ocean. The waters of the Central Indian Basin, east of the Southeast Indian Ridge and west of the Ninetyeast Ridge, have higher PALK concentrations, suggesting that these waters are older than waters to the east or west. Both the ^{14}C and PALK distributions suggest that the deep circulation is primarily controlled by topography. The main gap through which bottom waters can reach the Central Indian Basin is near the equator. A lesser gap exists at the southeast corner of the basin. Relatively

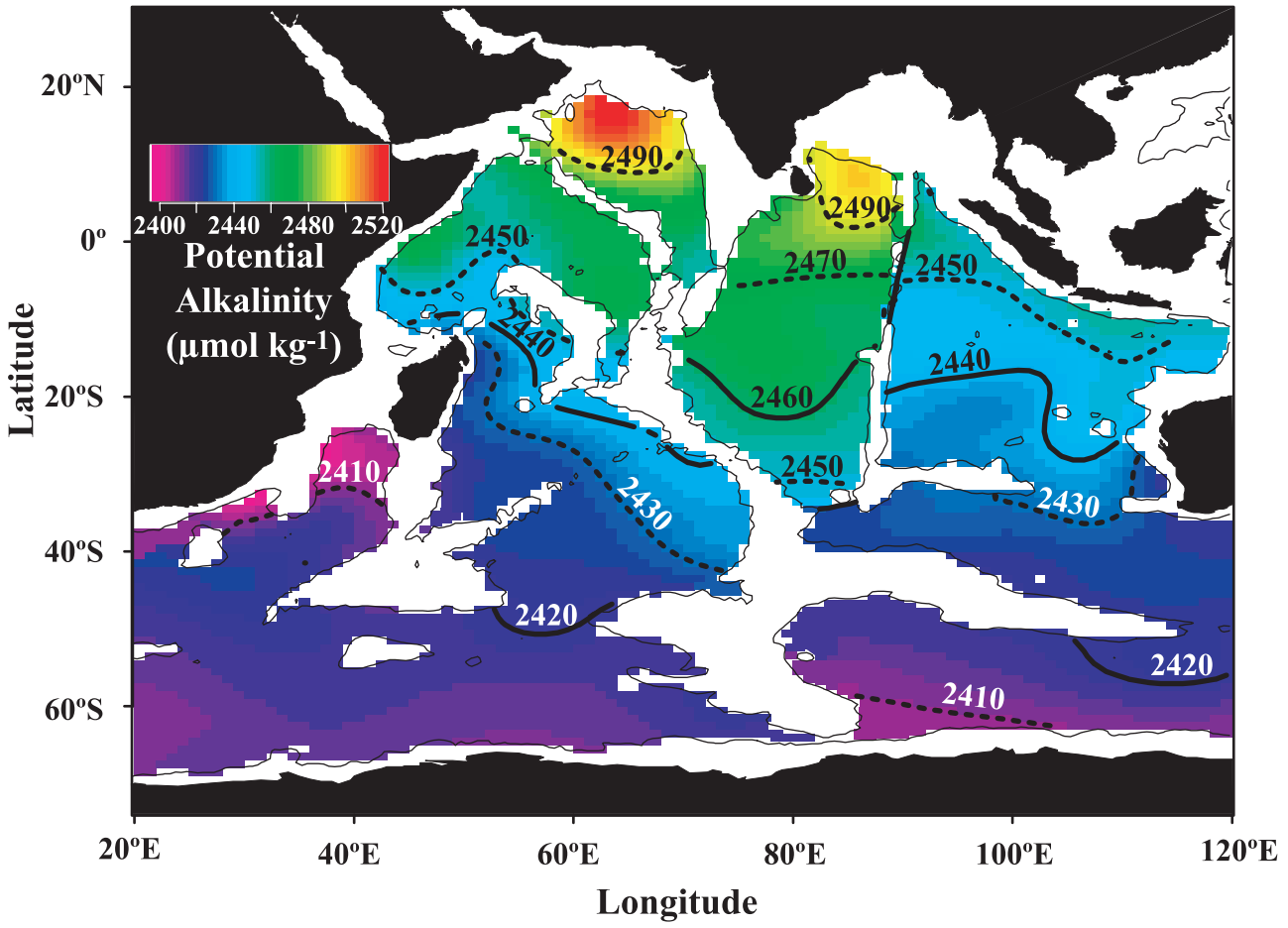

Figure 5. Map of PALK within 50 m of bottom where the bottom is >3500 m deep in the Indian Ocean. Thin lines indicate 3500-m contour. Symbols indicate station locations.

young waters coming through the lesser gap dilute the older waters that enter the Central Basin through the northern gap. The oldest waters appear to be at the northernmost end of the Indian Ocean, particularly in the Arabian Sea.

[16] Deep DIC concentrations can also be used to infer deep circulation. For example, *Goyet et al.* [1999] noted a local DIC minimum in the waters moving northward through the Owen Fracture zone at 9°N, 54°E, and 3500–4000 m. The bottom water DIC distribution (not shown) looks very similar to the PALK. The lowest bottom water values are observed off southeastern Africa and the highest values are found in the northern Arabian Sea.

[17] One area of interest with respect to deep water carbon distributions is the Andaman Sea, located in the northeastern Indian Ocean between the Maylayan Peninsula and the Andaman-Nicobar islands. The Andaman Sea is connected to the Bay of Bengal and shares similar shallow water characteristics. Below the sill depth at approximately 1300 m, however, several water properties diverge. *Sen Gupta et al.* [1981] and, more recently, *Sarma and Narvekar* [2001] noted that although the salinities are similar, the deep Andaman Sea waters are about 2°C warmer than the deep Bay of Bengal. They also observed higher nitrate and pCO_2 and lower silicate, oxygen, and alkalinity in the deep Andaman Sea relative to the same depths in the Bay of Bengal. These differences are attributed to low ventilation of the deep water because of the shallow sill depth [*Sen Gupta et al.*, 1981; *Sarma and Narvekar*, 2001].

[18] Similar features are observed with the WOCE/JGOFS data, but the chemistry of the deep waters clearly indicate a different source for the deep Andaman Sea waters compared to the deep Bay of Bengal. The observations are most consistent with the deep Andaman Sea waters originating from intermediate waters, with no direct influence from the northward-moving deep CDW observed in the bottom waters of the Bay of Bengal. Thus, low ventilation is not the primary reason for the observed differences. To evaluate in situ processes in the Andaman Sea one should not compare deep water properties inside and outside the Andaman Basin, but rather between sill depth water and deep Andaman water. Using salinity as a conservative tracer for comparing sill depth water in the Bay of Bengal with water at or below the sill depth in the Andaman Sea, we find that the silicate, DIC and TA are not significantly modified in the deep Andaman waters. Nitrate is slightly lower and oxygen slightly higher in the Andaman. This difference extends much shallower than the sill depth. *Sarma and Narvekar* [2001] suggested that the higher oxygen and pH values they observed near the oxygen minimum zone in the Andaman Sea was because that basin has lower rates of organic matter regeneration than the Bay of

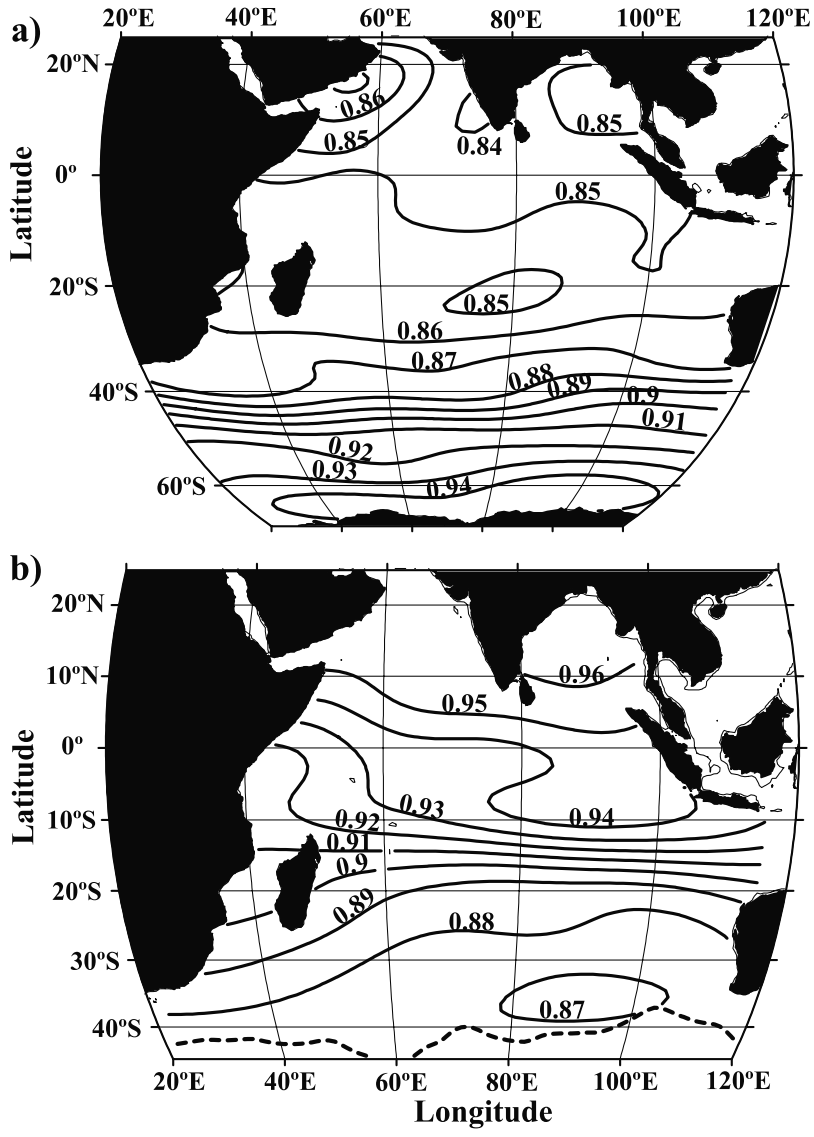

Figure 6. DIC/TA mapped (a) at the ocean surface and (b) on the surface where $\sigma_\theta = 26.0$. The dashed line at ~43°S in Figure 6b is the winter time outcrop of the density surface (based on *Levitus and Boyer* [1994] and *Levitus et al.* [1994]).

Bengal. This suggests that the deep Andaman Sea waters originate from within the Andaman Basin rather than a purely advective flow from the Bay of Bengal over the sill. Compared to the accumulated chemical signals in the deep Bay of Bengal, the deep Andaman Sea waters are relatively young and unaltered.

3.3. DIC/TA

[19] *Copin-Montegut* [1988, 1989] determined a method for calculating the effect of temperature changes on the partial pressure of CO_2 (pCO_2) in seawater based on the DIC to alkalinity ratio (DIC/TA). Since pCO_2 is frequently measured at some temperature other than the in situ temperature, this work improved the conversion to in situ conditions. *Goyet et al.* [1993] extended this concept using a more precise analytical technique. The basic result of these studies is that the temperature sensitivity of pCO_2 increases as DIC/TA approaches one. This change in sensitivity can affect the seasonal variations in air-sea CO_2 gas exchange. The DIC/TA also determines the buffer capacity of the oceans, which controls the efficiency of the oceanic sink for anthropogenic CO_2 [*Siegenthaler and Sarmiento*, 1993]. *Goyet et al.* [1999] described the DIC/TA distribution for a subset of the data used here (WOCE line I1). They noted that the highest surface ocean value along the section (0.86) was in the Arabian Sea near the coast of Somalia and the lowest (<0.84) between 68°E and 72°E just west of Sri Lanka. Surface values across the Bay of Bengal were approximately constant at 0.85. They also noted a shoaling of the 0.96 isoline from west to east across the Arabian Sea with little or no change in the isoline depth across the Bay of Bengal.

[20] A more interesting picture emerges when the entire basin is considered. Figure 6 shows the surface ocean distribution of DIC/TA. For this figure "surface" was taken

to mean the shallowest sample at each station so long as the sample pressure was less than or equal to 25 dbar. The most dominant feature by far is the more or less monotonic decrease in the ratio from 0.94 to 0.86 moving northward from the Southern Ocean into the main Indian Ocean basin. The DIC/TA ratio is reflecting the precipitous decrease in surface DIC from Antarctica to a basin minimum at approximately 10°S and a relatively small increase in TA from Antarctica to a local maximum at 30 to 35°S. North of this frontal region the only feature of note is the maximum found in the northern Arabian Sea off the coast of Yemen and Oman. This feature is a consequence of the southeast monsoon upwelling that brings high DIC/TA water up from below. The southern edge of this maximum is the feature noted by *Goyet et al.* [1999]. The ratio in Bay of Bengal surface waters is very slightly elevated relative to surface water south of the Bay. In spite of these two features, DIC/TA in main basin surface waters is remarkably constant (0.8541 ± .01; n = 1010).

[21] At a depth of only 50 dbar the pattern changes significantly. The value of the ratio still decreases strongly from the south (from >0.94 to <0.86), but reaches a minimum at approximately 20°S latitude. Northward from there in the eastern part of the basin the ratio increases fairly smoothly to a maximum >0.90 in the northern Bay of Bengal. Going northward in the western part of the basin the ratio first decreases to a relative minimum at the latitude of Somalia (~8°N) then increases strongly to maximum values of ~0.94 near the Yemen/Oman coast. A large part of the difference between these two surfaces is the density structure. This influence is apparent in Figure 6b where the ratio is mapped onto the potential density surface σ_θ =26.0. This surface outcrops near 42°S in the winter (dashed line based on work of *Levitus and Boyer* [1994] and *Levitus et al.* [1994],) has a maximum depth of ~250 m near 20°S and generally lies near 150 m north of there except in the northern Arabian Sea where it shoals to <100 m. On this density surface DIC/TA increases northward from the outcrop. Values in the Bay of Bengal are somewhat higher than in the Arabian Sea and the influence of Indonesian throughflow is evident as a kink in the 0.94 isoline (0–10°S, 80°W). The increasing ratio away from the outcrop is due to in situ decomposition of organic matter which simultaneously increases DIC and causes a slight decrease in TA.

[22] To demonstrate the strong meridional variability, Figure 7 shows sections for the upper kilometer of the water column in the eastern Indian Ocean (along ~93°E) plotted as a function of depth (Figure 7a) and potential density (Figure 7b). The general shape of the contours in the depth section is remarkably similar to the equivalent section of DIC concentration and, at first glance, not dissimilar to the equivalent TA section (Figure 2). Closer inspection of the concentrations shows that the strong vertical gradient in DIC dominates the relatively weak TA gradient, especially between latitudes 40°S and 20°S. This allows the DIC/TA section to mimic the DIC section so closely.

[23] The very strong meridional gradient with latitude at 15–20°S in Figure 7a is the "Chemical Front." *Wyrtki* [1973] attributed the chemical front to hydrography and circulation rather than local biogeochemical processes. The differences in circulation and stratification, however, also affect the local biological and geochemical cycles [e.g., *Sen Gupta and Naqvi*, 1984; *George et al.*, 1994]. South of the front the DIC/TA values are relatively constant along lines of constant potential density (Figure 7b). This structure suggests that advection and mixing has a strong effect on the ratios by transporting the surface DIC/TA values into the ocean's interior. North of the Chemical Front the DIC/TA values clearly increase at all densities, suggesting an increase in the relative importance of organic matter decomposition in the northern Indian Ocean. The distribution of apparent oxygen utilization (AOU) is also very similar to the DIC and DIC/TA sections. AOU increases over lines of constant potential density (not shown) are much more dramatic north of the chemical front than in the southern Indian Ocean. Higher biological productivity and increased stratification north of the Chemical Front contribute to these phenomena. The trend toward higher DIC/TA makes the waters north of the front more corrosive to carbonate minerals than the southern waters. This will be examined further in later sections.

[24] Relative to the meridional sections, the zonal sections of DIC/TA are rather monotonous. The I1 section at ~10°N was described by *Goyet et al.* [1999]. The relatively higher subsurface ratios in the Bay of Bengal will tend to make the eastern waters more corrosive to carbonate minerals than the Arabian Sea waters. Examined in potential density space (similar to Figure 7b) the upper kilometer of the I2 section at ~8°S (not shown) exhibits a monotonic shoaling of DIC/TA isolines from west to east, but for any given potential density level the total cross basin change in the ratio is ≤0.01. For the upper kilometer of the I3 section at 20°S (not shown), the DIC/TA isolines at depths where the potential density is >26.6 are essentially flat across the entire basin. Isolines occurring at lighter densities are flat across the center of the basin, but turn upward near Australia and Madagascar. These gradients are presumably due to the near shore current(s) in both areas.

[25] The zonal DIC/TA structure becomes much more complicated in the Southern Ocean section, S4I at ~62.5°S. The subsurface DIC/TA is relatively high, as in the northern Indian Ocean, with a rather narrow range (0.94 to 0.97 for the entire section). Figure 8 shows DIC/TA in potential density space for the upper kilometer. In general, the ratio increases with density (and depth) to the σ_θ = 27.6 level, then decreases below that. There is a discontinuity in the pattern at ~90°E which coincides with the location of the Kerguelen Ridge. This pattern break continues to the bottom and is caused by circulation and topography [e.g., *Mantyla and Reid*, 1983; *Haine et al.*, 1998]. In the bottom waters, the Kerguelen Ridge separates waters which have characteristics of the Weddell Sea on the west side from those with Ross Sea characteristics on the east side of the ridge.

[26] When the entire Indian Ocean region is considered, the best description of the DIC/TA ratio for deep and bottom waters is that it is almost constant. From 2000 dbar to the bottom the ratio gradually decreases from ~0.96 to ~0.953; however, the mean of all measurements for this water is 0.9549 ± 0.0039 (σ_m = 0.00005; n = 6133). This is not to say that DIC and TA are not changing in the deep

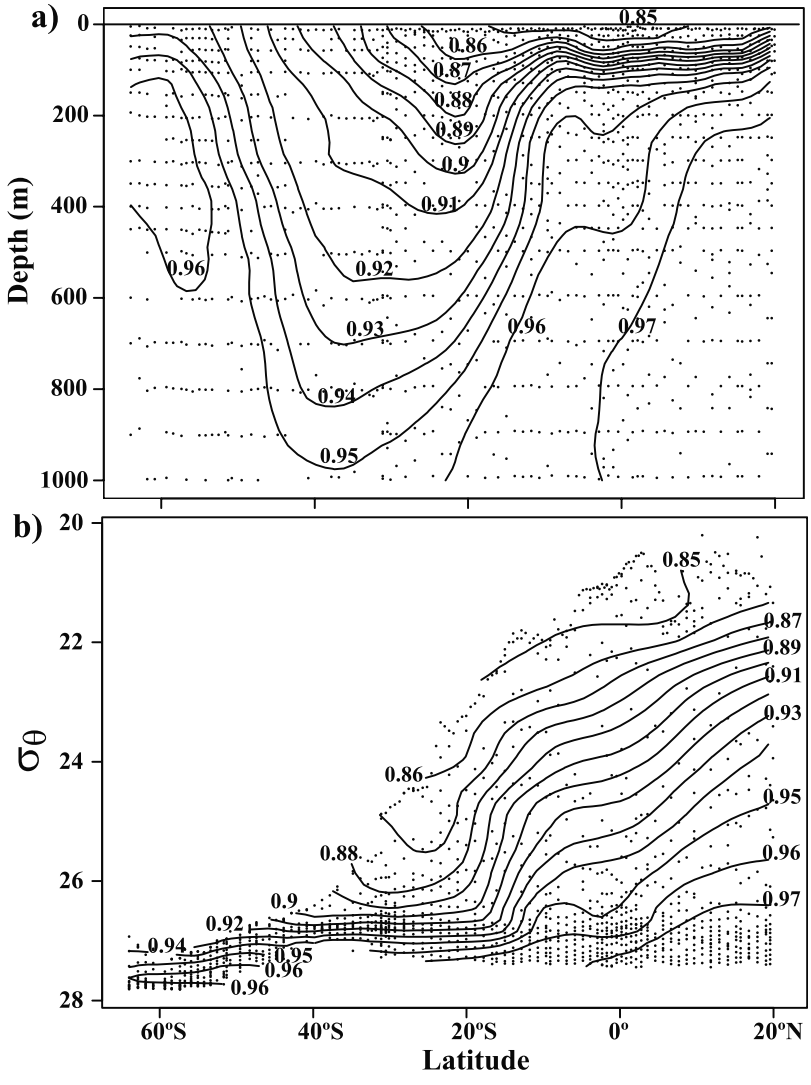

Figure 7. Vertical section in (a) depth and (b) potential density space for DIC/TA in the upper kilometer of the water column along ~92°E.

waters, but that the changes are of roughly similar magnitudes. One exception to the deep water consistency is the relatively low DIC/TA values in the deep waters near the South African coast. As noted in the PALK map (Figure 5), relatively young NADW comes around the southern tip of Africa and moves north along the coast [*Toole and Warren*, 1993]. These waters clearly show up as low DIC/TA values in the deep and bottom waters at the western end of the I3 section.

[27] The sharp increases in DIC/TA from the surface to intermediate waters result from both the translation of the surface gradients observed in Figure 6a into the ocean interior and a dominance of organic matter remineralization over carbonate dissolution (note increase in DIC/TA along isopycnal surface in Figure 6b). In the deep waters there is less organic matter to remineralize and DIC/TA ratios are much more consistent. The increase in intermediate and deep DIC/TA values to the north makes the saturation state of the waters with respect to carbonate minerals more favorable for dissolution. The DIC/TA ratios, however, do not directly indicate where in the water column carbonate dissolution is occurring. In the next section we will examine the carbonate system of the Indian Ocean.

4. Carbonate Cycling

4.1. $CaCO_3$ Dissolution and Saturation Depths

[28] One of the important processes controlling the concentration of DIC and TA in both near surface and deep ocean waters is the formation and dissolution of $CaCO_3$ tests. In near surface waters plankton convert dissolved bicarbonate ions to $CaCO_3$ and dissolved carbon dioxide. In deep water some of the $CaCO_3$ dissolves and the remainder is buried in the sediment. Practically all of the pelagic carbonate sediments consists of calcitic foraminifera and coccolith debris; however, *Berner* [1977] argued that approximately as much $CaCO_3$ in the form of aragonite (as pteropod tests) was formed in surface waters as calcite. The lack of aragonitic sediments in deeper waters is simply due to the fact that aragonite is much more soluble than calcite.

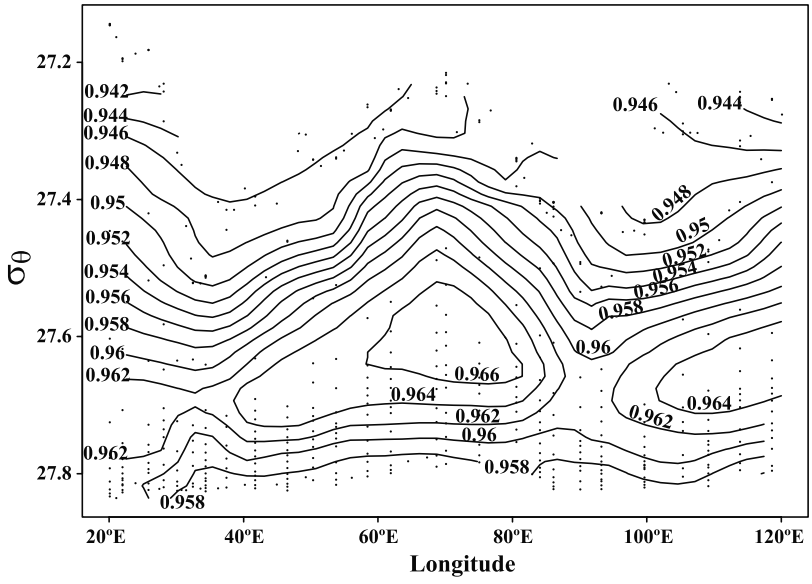

Figure 8. DIC/TA section in potential density space for the upper kilometer of the S4I section at ~62.5°S. Points indicate sample locations.

[29] It is well known that as the depth increases in the ocean, the degree of saturation with respect to both calcite and aragonite decreases. The level at which $CaCO_3$ is in thermodynamic equilibrium with respect to dissolution is known as the saturation depth. This depth is not the same as the lysocline and is significantly different for calcite and aragonite due to the solubility difference. Given the constants and relationships referenced and/or listed in section 2.2 it is possible to estimate the saturation depth for aragonite and calcite from the TA and DIC data. Figure 9 shows the saturation depth in meters for aragonite (Figure 9a) and calcite (Figure 9b). For the entire basin, including the southern sector, the average calcite saturation depth is 3621 ± 307 m (σ_m = 14; n = 463) and the range is approximately 2900–3900 m. In both the Arabian Sea and Bay of Bengal the calcite saturation depth is less than 3000 m at the northern extremes. These saturation depths are somewhat deeper than previous estimates [e.g., *Sen Gupta and Naqvi*, 1984; *Anderson and Dyrssen*, 1994; *George et al.*, 1994] that suggested that calcite saturation depths were as shallow as 1500 m in the northern Arabian Sea. However, the extensive WOCE/JGOFS data set provides a much better base for evaluating these trends. These results are consistent with the more recent study of *Mintrop et al.* [1999]. A thorough discussion of the reasons for the discrepancies is presented by Mintrop. The results presented here are also more consistent with the saturation horizons of other basins [e.g., *Feely et al.*, 2002].

[30] The average saturation depth for aragonite is 836 ± 337 m (σ_m = 15; n = 534) and the range is approximately 200–1400 m. Although the span of calcite and aragonite saturation depths is similar (~1000 m), the saturation horizon shapes are very different. The deepest calcite saturation depth is in the central Indian Ocean with rapid shoaling at the northern and southern boundaries. The deepest aragonite saturation, on the other hand, is in the southwestern Indian Ocean. The saturation horizon then shoals toward the northeast to a minimum of 200–400 m in the Bay of Bengal.

[31] The aragonite saturation depths are shallow enough to have been affected by anthropogenic CO_2 (Figure 4). South of ~30°S, aragonite saturation depths based on the preindustrial DIC concentrations are nearly the same as today. North of 30°S, however, the current 100% saturation depth becomes progressively shallower than the preindustrial depth. In the northern Arabian Sea and Bay of Bengal, the current aragonite saturation depths are 100 and 200 m shallower, respectively, than in preindustrial times. Therefore, the preindustrial Arabian Sea and the Bay of Bengal aragonite saturation depths were more similar than today. The northward shoaling in the Indian Ocean is somewhat larger than estimated for the North Pacific because the anthropogenic CO_2 concentrations at these depths are greater in the Northern Indian Ocean than in the North Pacific [*Sabine et al.*, 1999; *Feely et al.*, 2002; *Sabine et al.*, 2002]. Shoaling of the saturation horizons means that carbonate particles settling through the water column will begin to dissolve at shallower depths, neutralizing some of the anthropogenic CO_2 and possibly decreasing the supply of particles to the sediments.

[32] *Berner* [1977] produced a global map of pteropod ooze (aragonite) sediments based on the data of *Murray and Chumley* [1924], *Chen* [1964], and *Herman* [1971]. For the Indian Ocean only four small zones were indicated: (1) the northern Arabian Sea near the mouth of the Persian Gulf, (2) southwest of the southern tip of India centered on ~75°E, (3) along the eastern coast of Tanzania, and (4) northeast of the northern tip of Madagascar (Seychelles plateau). On the basis of the saturation depth and topography in Figure 9a, none of these regions would have been predicted. The difference may indicate areas of unusually high pteropod abundance or more likely be evidence of turbadite flow. The shoaling of the aragonite saturation

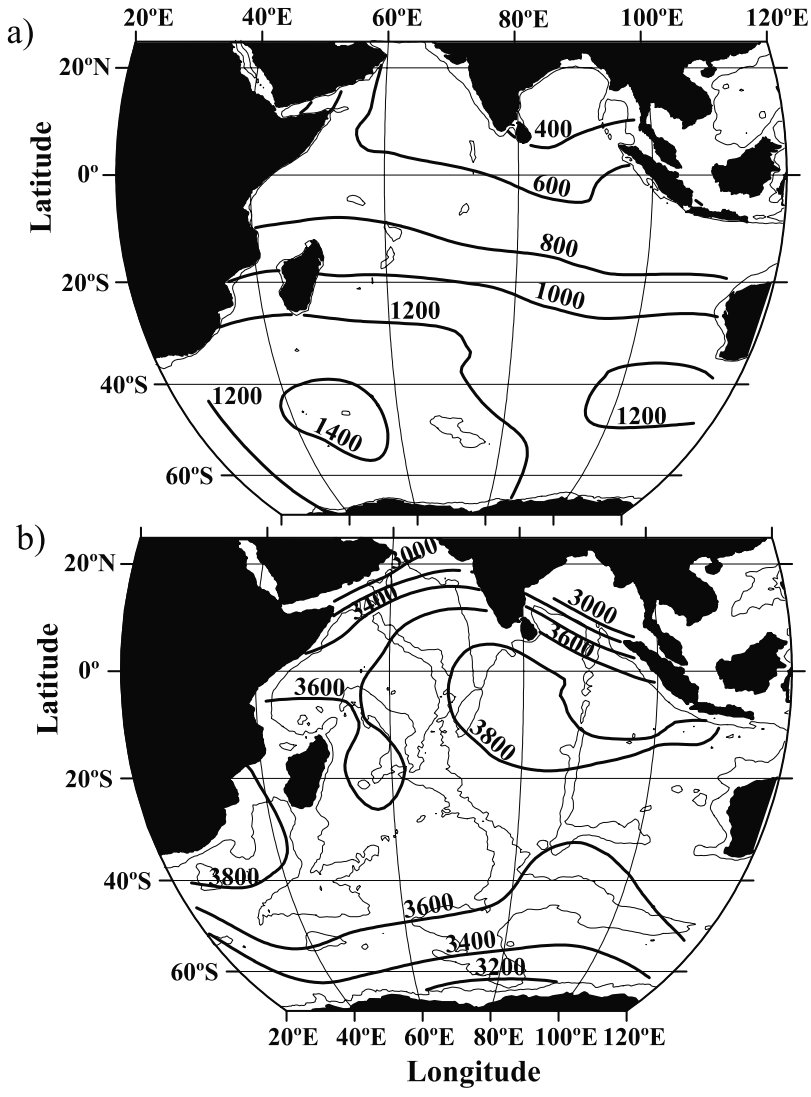

Figure 9. Saturation depth in meters for (a) aragonite and (b) calcite estimated from estimated water column DIC and TA concentrations. The 800-m bathymetry is indicated for aragonite, and the 3500-m bathymetry is indicated for calcite.

horizons due to invasion of anthropogenic CO_2 will tend to dissolve sediments in these areas if the occurrence is due to production, but would not have much influence on turbadite flows due to rapid burial. *Lisitzin* [1972, Figure 128, p. 140] published a global map of the calcium carbonate (primarily calcite) distribution in the sediments. The carbonate sediments are, as expected, primarily along the shallower topography associated with the oceanic ridge systems in the Indian Ocean and are especially abundant in the 40°–50°S latitude band. His estimate of the carbonate compensation depth (point at which calcite is no longer found in the sediments) is, as expected, deeper than the saturation depths shown in Figure 9b.

[33] Most of the intermediate and deep waters in the Indian Ocean and the South Pacific Ocean are slightly undersaturated with respect to aragonite and slightly oversaturated with respect to calcite. This causes a large separation between the aragonite and calcite saturation depths. In these areas, the calcite saturation horizons are sufficiently deep to have not been affected yet by anthropogenic CO_2. As anthropogenic CO_2 continues to accumulate in the shallow and intermediate waters of the Indian and South Pacific oceans it is conceivable that the intermediate waters could become undersaturated with respect to calcite while deeper water remains oversaturated with respect to calcite. This situation is not likely to occur in the North Pacific. North Pacific waters are slightly more corrosive than the waters of the South Pacific or Indian Ocean. This difference, however, is spread throughout most of the water column and is sufficient to dramatically shoal the calcite saturation depth in the North Pacific. Anthropogenic CO_2 in this region will only serve to shoal the existing calcite saturation horizon further.

4.2. TA* Distributions

[34] Using the TA* approach described in section 2.2, we can estimate the mass of carbonate that has dissolved in the

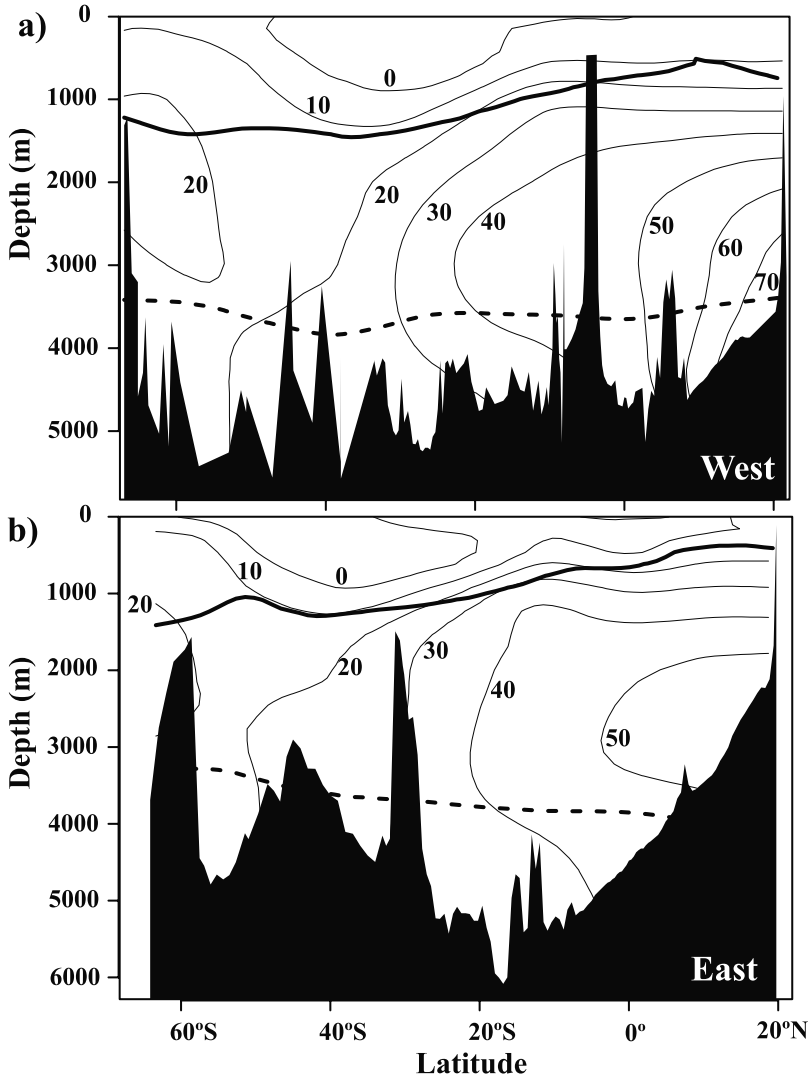

Figure 10. Sections of TA* (μmol kg^{-1}) in (a) the west and (b) the east. Thick solid line indicates depth of aragonite saturation horizon. Thick dashed line indicates depth of calcite saturation horizon.

Indian Ocean. Evidence of dissolution at shallow depths can be seen in meridional sections of TA* (Figure 10). The dissolution begins much shallower than the 100% saturation horizon for calcite, but very near the saturation horizon for aragonite. These findings are consistent with *Anderson and Dyrssen* [1994], *Mintrop et al.* [1999], and *Sarma and Narvekar* [2001], who suggested that significant carbonate dissolution occurred at 400–600 m and below in the northern Indian Ocean. This is also consistent with calcium to chlorinity ratios which show low values at the surface, then a steady increase with depth below approximately 200 m [*Sen Gupta et al.*, 1978]. The calcium to chlorinity ratios from the northern Indian Ocean are appreciably higher than oceanic averages [*Sen Gupta and Naqvi*, 1984]. Although Sen Gupta and Naqvi attribute some of this calcium to river inputs into the Northern Indian Ocean, the lack of enrichments in other measured species led them to conclude that the observed calcium profiles are best explained by excessive stripping of calcium from surface waters by high biological activity and its subsequent remineralization at depth.

[35] One can get a qualitative sense of where carbonate dissolution is occurring by examining the average profiles of TA* as a function of distance above the bottom (Figure 11). To minimize aliasing from shallow coastal waters, profiles only consider data with bottom depths >2000 m. The Southern Ocean profile shows the dissolution signal that is transported in as part of the CDW. The signal is less than 20 μmol kg^{-1} and is well mixed through the intermediate and deep waters. As the deep waters start moving north into the southern Indian Ocean (50° to 20°S) they begin accumulating alkalinity. A very slight mid-depth maximum develops in the profiles as one moves north. North of the Chemical Front, values are 20 to 30 μmol kg^{-1} higher than Southern Ocean values. The mid-depth maximum is very pronounced. Although there is a mid-depth southward flow of old waters, the TA* maximum is located at a different depth and is much more distinct than the ^{14}C minimum. These differences

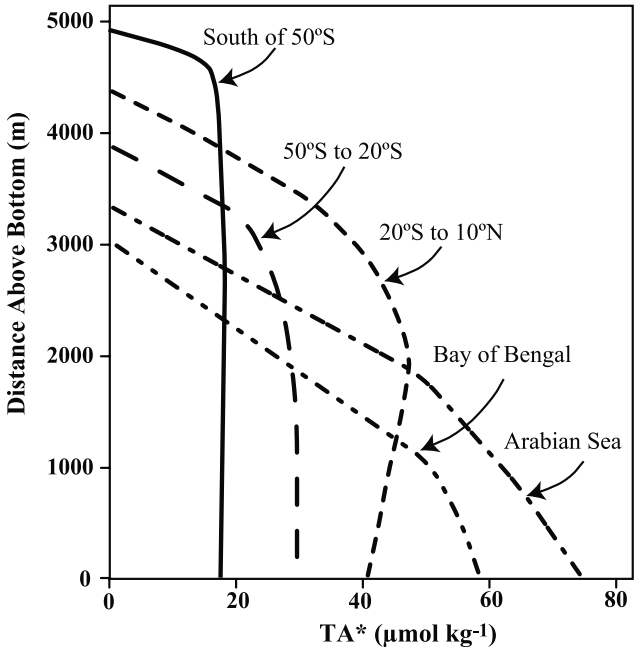

Figure 11. Average profiles of TA* as a function of distance above the bottom (where bottom depth is >2000 m) for different regions of the Indian Ocean.

suggest that the alkalinity signal is dominated by local dissolution processes in the water column rather than simple transport. The Bay of Bengal and the Arabian Sea, however, show maximum TA* values closest to the sea floor. These profiles are consistent with a strong benthic source of alkalinity. The Arabian Sea has the highest dissolution signal, with values up to 60 µmol kg^{-1} above Southern Ocean values. Both the Bay of Bengal and the Arabian Sea show a change in the rate of decrease in TA* as distance above the bottom increases. The slope change for the Bay of Bengal is about 1000 m off the bottom. It is clearly shallower in the Arabian Sea. The slopes at all depths appear to be greater in the Bay of Bengal. These differences may be attributed to either the profoundly different biogeochemical cycling in the Bay of Bengal versus the Arabian Sea [e.g., *George et al.*, 1994], or to the differing paths for the deep water sources through these two areas (e.g., Figure 5). To quantitatively evaluate where in the water column the dissolution is occurring, one must use a watermass age tracer.

4.3. $CaCO_3$ Dissolution Rate Estimates

[36] The radioactive decay of natural ^{14}C (1% every 83 years) in the deep waters of the Indian Ocean can be used together with the TA* to estimate an overall $CaCO_3$ dissolution rate for the deep ocean. For waters with no bomb ^{14}C contamination (depths >1500 m) the average dissolution rate is 0.06 µmol kg^{-1} yr^{-1} ($r^2 = 0.81$, n = 663). This rate is higher than comparable estimates in the Pacific or Atlantic Oceans [*Feely et al.*, 2002]. To determine the spatial variability of the deep-water dissolution rates, these data were subsetted into data north of the Chemical Front (at 20°S) and south of the front, then examined on isopycnal surfaces. Unfortunately, there were not enough data to get reliable estimates for the Bay of Bengal or the Arabian Sea individually. The rates of dissolution in the south decrease slowly from 0.055 to 0.045 µmol kg^{-1} yr^{-1} with increasing density, but then drop rapidly in the two deepest surfaces examined (Figure 12). In the northern Indian Ocean the dissolution rates are only slightly lower than the southern Indian values at the lowest density, but then decrease to a minimum of 0.017 µmol kg^{-1} yr^{-1} at a potential density (referenced to 3000 dbars; σ_3) of 41.05. The dissolution rate increases to a maximum value of 0.083 µmol kg^{-1} yr^{-1} at a σ_3 of 41.25. This increase is coincident with the depth of the calcite saturation horizon. At $\sigma_3 > 41.25$ the rates decrease with increasing density. The exact cause of the differing profiles north and south of the Chemical Front is not clear, but may be related to the apparent dominance of a sedi-

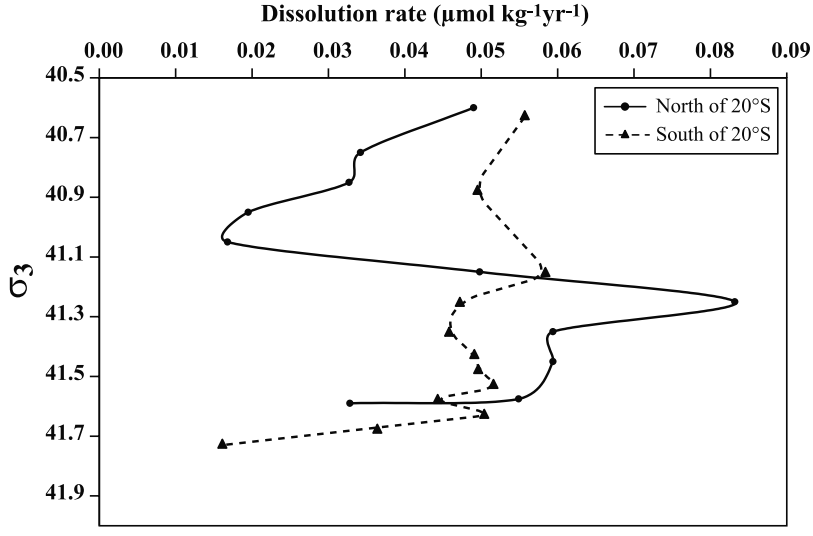

Figure 12. Plot of dissolution rate as a function of σ_3 (potential density referenced to 3000 dbar) for deep Indian Ocean data.

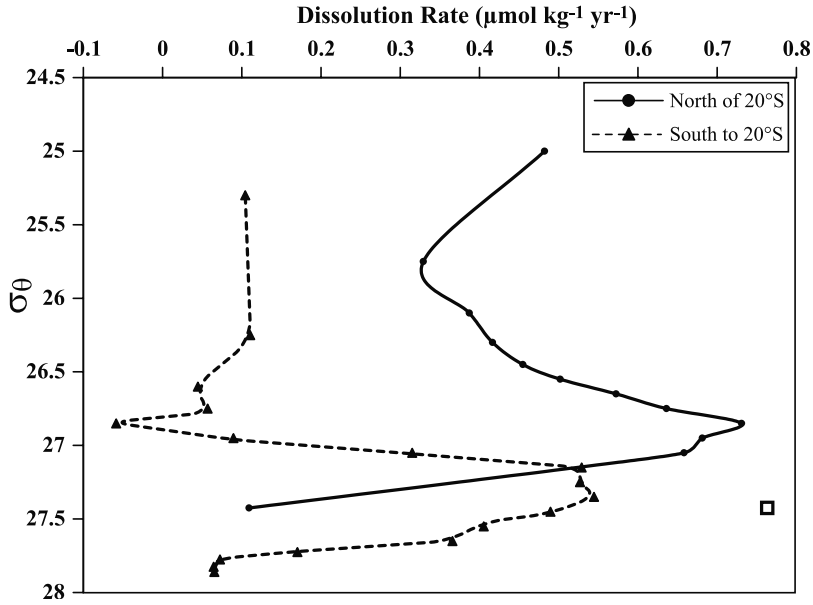

Figure 13. Plot of dissolution rate as a function of σ_θ (potential density referenced to the surface) for shallow Indian Ocean data. The solid line is from data north of 20°S (excluding data from the Bay of Bengal and the Gulf of Oman) and the dashed line is from data south of 20°S. The open square symbol shows the implied dissolution rate if the Gulf of Oman data are included.

mentary alkalinity source in the north as opposed to the middepth dissolution signal in the south. The fact that the northern profile shows a dissolution peak that is coincident with the calcite saturation horizon is consistent with the sedimentary record that shows more calcite preserved in the sediments in the southern Indian Ocean [*Lisitzin*, 1972]. More work is needed to confirm this observation and investigate the processes controlling sedimentary versus water column sources of alkalinity to the deep ocean.

[37] The use of ^{14}C as an age tracer is limited to the deep water because of contamination with bomb ^{14}C near the surface. To examine dissolution rates shallower than 1500 m we use CFC-11 as an age tracer. As with the ^{14}C analysis, the TA* data were divided into points north and south of the Chemical Front at ~20°S and analyzed on isopycnal surfaces. The shallow data have the added complication that the preformed alkalinity estimates in the Bay of Bengal are not valid because of the higher TA/salinity from the river water (see Figure 3b). The net result of this bias would be dissolution estimates that are biased high. To minimize this bias all of the data in the Bay of Bengal (north of 9°N) were excluded from these calculations.

[38] Dissolution rates in the upper water column are up to an order of magnitude higher than the deep dissolution rates (Figure 13). In the southern Indian Ocean there is little evidence of dissolution in waters with potential densities less than $\sigma_\theta = 26.9$ (mean depth ~800 m). At $\sigma_\theta > 26.9$ the dissolution rates increase dramatically to a maximum of ~0.52 μmol kg^{-1} yr^{-1} at $\sigma_\theta = 27.2 - 27.4$ (roughly 1200 m depth). The rates quickly drop back down to <0.1 μmol kg^{-1} yr^{-1} at higher densities. The depth of the maximum dissolution rate is just below the calculated saturation depth for aragonite.

[39] Dissolution rates north of 20°S are generally higher than the rates to the south (Figure 13). A maximum rate of 0.73 μmol kg^{-1} yr^{-1} is observed at $\sigma_\theta = 26.9$, significantly shallower than the southern maximum. This shoaling, however, is consistent with a shoaling of the aragonite saturation horizon in the northern Indian Ocean. Below $\sigma_\theta = 26.9$, the rates decrease to ~0.1 μmol kg^{-1} yr^{-1}. The values at the highest densities are consistent with the estimates from the deep ocean using the ^{14}C approach. The two techniques do not quite overlap because the CFC-11 ages are only reliable to ~30 years, limiting the maximum density that can be examined.

[40] These data suggest that there is significant calcium carbonate dissolution at relatively shallow depths in the Indian Ocean. This dissolution is most likely occurring in the water column since most of these data were collected well away from the coast with bottom depths much deeper than this method can address. The fact that the dissolution rates increase dramatically just below the aragonite saturation depth and even shoal to the north in the same manner as the aragonite saturation horizon, lends support to *Berner*'s [1977] suggestion that there is significant aragonite production in the Indian Ocean that is not preserved in the sediments. These findings are also supported by several other recent studies [*Mintrop et al.*, 1999; *Sarma and Narvekar*, 2001] that found substantial dissolution well above the calcite lysocline. Other mechanisms, including dissolution of $CaCO_3$ in the guts of zooplankton [e.g., *Pond et al.*, 1995], enhanced dissolution of $CaCO_3$ particles in microenvironments where bacterial oxidation is occurring [e.g., *Jansen and Wolf-Gladrow*, 2001], or dissolution of more soluble carbonate phases [e.g., *Sabine and Mackenzie*, 1995] may also contribute to the observed mid water signal.

[41] Although the northern Indian Ocean is bounded on three sides by land, there are additional water sources to this region that must be accounted for. In particular, the Red Sea and Persian Gulf are sources of high salinity, high alkalinity water that enter the Arabian Sea at intermediate depths [e.g., *Anderson and Dyrssen*, 1994]. This water enters the Arabian Sea through the Gulf of Aden and Gulf of Oman with σ_θ values near the largest densities in Figure 13. The rates given for the σ_θ = 27.4 have excluded data from these regions to better reflect the overall dissolution rate for the northern Indian Ocean. If the data from these gulfs were included, the inferred dissolution rate would be 0.76 μmol kg^{-1} yr^{-1} (see Figure 13). The anomalously high rate estimates for these samples may result from inappropriate preformed alkalinity estimates for the Red Sea and Persian Gulf waters or from an imported signal of dissolution from these regions. Either way, the lower rate determined by excluding these few samples near the mouths of the Red Sea and Persian Gulf should be more indicative of the local northern Indian Ocean dissolution rates. Other sources of alkalinity not considered here, such as noncarbonate related sedimentary sources of TA [e.g., *Chen*, 2002], may also affect these results and need to be examined further.

5. Conclusions

[42] The distribution of DIC and TA in the Indian Ocean is controlled by the large-scale circulation patterns and the strength of the biological pump. Intermediate and deep water DIC and TA concentrations in the Indian Ocean generally lie between the Atlantic and Pacific concentrations. Shallow DIC concentrations have increased by as much as 50 μmol kg^{-1} because of the invasion of anthropogenic CO_2. The penetration of anthropogenic CO_2 into the ocean's interior has been documented and is serving to decrease the vertical DIC gradient. Standard thinking is that the TA concentration in the ocean is not affected by anthropogenic CO_2. However, anthropogenic CO_2 has penetrated deep enough to shoal the aragonite saturation horizons by as much as 33% in the northern Indian Ocean. It is not possible to determine at this point whether the alkalinity budget of the ocean has, in fact, changed as a result of anthropogenic CO_2. But, aragonite saturation horizons will shoal even more in the future as ocean DIC inventories continue to increase. Injection of anthropogenic CO_2 at the surface could also generate calcite saturation profiles that are not currently observed in today's oceans, with waters that are undersaturated with respect to calcite overlying oversaturated waters.

[43] The total amount of $CaCO_3$ that is currently dissolved in the Indian Ocean can be determined by integrating TA* throughout the water column. To remove the contribution from dissolution outside of the Indian basin that is transported in with the deep and intermediate waters, all values were normalized to the average concentrations south of 35°S. The total inventory of $CaCO_3$ that has dissolved within the Indian Ocean north of 35°S is 34 Pg C. This would imply an average dissolution rate of ~0.1 Pg C yr^{-1} based on a mean ^{14}C age of 280 years for intermediate and deep waters. Although this is a very crude calculation it is generally consistent with a piecewise integration of the isopycnal rate estimates. The total inventory is approximately 20% of the Pacific inventory, with an estimated dissolution rate that is roughly one third of the Pacific rate [*Feely et al.*, 2002]. The isopycnal dissolution rates have a lot of structure with local maxima occurring in intermediate waters just below the aragonite saturation horizon. Dissolution is also generally higher north of the Chemical Front. There is some evidence for significant sedimentary sources of alkalinity in the Bay of Bengal and the Arabian Sea.

[44] These results generally support the recent suggestion by *Milliman et al.* [1999] that significant dissolution of carbonate minerals occurs in the water column well above the calcite lysocline. The exact mechanisms that promote this dissolution still need further investigation, but the water chemistry analyses are consistent with a rapid dissolution of aragonite particles just below the aragonite saturation horizon.

[45] **Acknowledgments.** We wish to acknowledge all of those that contributed to the Indian Ocean data set compiled for this project, including those responsible for the carbon measurements, the CFC measurements, and the Chief Scientists. This work was funded by NOAA/DOE grant GC99-220, NSF grants OCE-9818877 and OCE-0137144, and the Joint Institute for the Study of the Atmosphere and Ocean (JISAO) under NOAA Cooperative Agreement NA17RJ1232. We thank Lisa Dilling of the NOAA Office of Global Programs and Donald Rice of the National Science Foundation for their efforts in the coordination of this study. JISAO Contribution 899 and PMEL contribution 2450.

References

Aller, R. C., Carbonate dissolution in nearshore terrigenous muds: The role of physical and biological reworking, *J. Geol.*, *90*, 79–95, 1982.

Anderson, L., and D. Dyrssen, Alkalinity and total carbonate in the Arabian Sea: Carbonate depletion in the Red Sea and Persian Gulf, *Mar. Chem.*, *47*, 195–202, 1994.

Archer, D., and E. Maier-Reimer, Effect of deep-sea sedimentary calcite preservation on atmospheric CO_2 concentration, *Nature*, *367*, 260–263, 1994.

Berner, R. A., Sedimentation and dissolution of pteropods in the ocean, in *The Fate of Fossil Fuel CO_2 in the Oceans*, edited by N. R. Andersen and A. Malahoff, pp. 243–260, Plenum, New York, 1977.

Bramlette, M. N., Pelagic Sediments, in *Oceanography*, Publ. 67, edited by M. Sears, 345–366, Am. Assoc. for the Adv. of Sci., Washington, D.C., 1961.

Brewer, P. G., Direct observation of the oceanic CO_2 increase, *Geophys. Res. Lett.*, *5*, 997–1000, 1978.

Brewer, P. G., and J. C. Goldman, Alkalinity changes generated by phytoplankton growth, *Limnol. Oceanogr.*, *21*, 108–117, 1976.

Brewer, P. G., G. T. F. Wong, M. P. Bacon, and D. W. Spencer, An oceanic calcium problem?, *Earth Planet. Sci. Lett.*, *26*, 81–87, 1975.

Broecker, W. S., "NO", a conservative water-mass tracer, *Earth Planet Sci. Lett.*, *23*, 100–107, 1974.

Broecker, W. S. and T. Takahashi, Neutrilization of fossil fuel CO_2 by marine calcium carbonate, in *The Fate of Fossil Fuel CO_2 in the Oceans*, edited by N. R. Anderson and A. Malahoff, pp. 213–241, Plenum, New York, 1977.

Chen, C., Pteropod ooze from Bermuda Pedestal, *Science*, *144*, 60–62, 1964.

Chen, C.-T. A., Self vs. dissolution-generated alkalinity above the chemical lysocline, *Deep Sea Res., Part II*, in press, 2002.

Chen, C.-T. A., and F. J. Millero, Gradual increase of oceanic CO_2, *Nature*, *277*, 205–206, 1979.

Chen, C.-T. A., R. M. Pytkowicz, and E. J. Olson, Evaluation of the calcium problem in the south Pacific, *J. Geochem.*, *16*, 1–10, 1982.

Copin-Montegut, C., A new formula for the effect of temperature on the partial pressure of CO_2 in seawater, *Mar. Chem.*, *25*, 29–37, 1988.

Copin-Montegut, C., Corrigendum, *Mar. Chem*, *27*, 143–144, 1989.

Corry, C., et al., Requirements for WOCE Hydrographic Programme data reporting, edited by T. Joyce and C. Corry, *WHPO Publ. 90-1 Rev. 2*, 145 pp., WOCE Hydrograph. Programme Off., La Jolla, Calif., 1994.

Department of Energy, *Handbook of Methods for the Analysis of the Various Parameters of the Carbon Dioxide System in Sea Water* version 2, edited by A. G. Dickson and C. Goyet, Washington, D.C., 1994.

Dickson, A. G., The ocean carbon dioxide system: Planning for quality data, *US JGOFS News*, *2*(2), 2, 1990.

Dickson, A. G., and F. J. Millero, A comparison of the equilibrium constants for the dissociation of carbonic acid in seawater media, *Deep Sea Res.*, *34*, 1733–1743, 1987.

Dickson, A. G., and J. P. Riley, The estimation of acid dissociation constants in seawater from potentiometric titrations with strong base, I, The ion product of water-K_W, *Mar. Chem.*, *7*, 89–99, 1979.

Dickson, A. G., G. C. Anderson, and J. D. Afghan, Reference materials for oceanic CO_2 analysis, 1, Preparation, distribution, and use, *Mar. Chem.*, in press, 2002a.

Dickson, A. G., J. D. Afghan, and G. C. Anderson, Reference materials for oceanic CO_2 analysis, 2, A method for the certification of total alkalinity, *Mar. Chem.*, in press, 2002b.

Feely, R. A., et al., In situ calcium carbonate dissolution in the Pacific Ocean, *Global Biogeochem. Cycles*, in press, 2002.

Fine, R. A., Circulation of Antarctic Intermediate water in the South Indian Ocean, *Deep Sea Res., Part I*, *40*, 2021–2042, 1993.

George, M. D., M. D. Kumar, S. W. A. Naqvi, S. Banerjee, P. V. Narvekar, S. N. de Sousa, and D. A. Jayakumar, A study of the carbon dioxide system in the northern Indian Ocean during premonsoon, *Mar. Chem.*, *47*, 243–254, 1994.

Goyet, C., F. J. Millero, A. Poisson, and D. K. Shafer, Temperature dependence of CO_2 fugacity in seawater, *Mar. Chem.*, *44*, 205–219, 1993.

Goyet, C., C. Coatanoan, G. Eischeid, T. Amaoka, K. Okuda, R. Healy, and S. Tsunogai, Spatial variation of total CO_2 and total alkalinity in the northern Indian Ocean: A novel approach for the quantification of anthropogenic CO_2 in seawater, *J. Mar. Res.*, *57*, 135–163, 1999.

Haine, T. W. N., A. J. Watson, M. I. Liddicoat, and R. R. Dickson, The flow of Antarctic bottom water to the southwest Indian Ocean estimated using CFCs, *J. Geophys. Res.*, *103*(C12), 27,637–27,653, 1998.

Herman, Y., Vertical and horizontal distribution of pteropods in quarternary sequences, in *The Micropaleontology of Oceans*, edited by B. M. Funnell and W. R. Riedel, pp. 3–74, Cambridge Univ. Press, New York, 1971.

Jansen, H., and D. A. Wolf-Gladrow, Carbote dissolution in copepod guts, *Mar. Ecol Prog. Ser.*, *221*, 199–207, 2001.

Johnson, K. M., A. E. King, and J. M. Sieburth, Coulometric TCO_2 analyses for marine studies: An introduction, *Mar. Chem.*, *16*, 61–82, 1985.

Johnson, K. M., et al., Coulometric total carbon dioxide analysis for marine studies: Assessment of the quality of total inorganic carbon measurements made during the US Indian Ocean CO_2 Survey 1994–1996, *Mar. Chem.*, *63*, 21–37, 1998.

Khoo, K. H., R. W. Ramette, C. H. Culberson, and R. G. Bates, Determination of hydrogen ion concentrations in seawater from 5 to 40°C: Standard potentials at salinities from 20 to 45‰, *Anal. Chem*, *49*, 29–34, 1977.

Levitus, S., and T. P. Boyer, Temperature, in *NOAA Atlas NESDIS 3: World Ocean Atlas 1994*, *NOAA Tech. Rep. 3*, Environ. Satell. Data and Inf. Serv., Silver Spring, Md., 1994.

Levitus, S., R. Burgett, and T. P. Boyer, Salinity, in *NOAA Atlas NESDIS 3: World Ocean Atlas 1994*, *NOAA Tech. Rep. 3*, Environ. Satell. Data and Inf. Serv., Silver Spring, Md., 1994.

Lewis, E., and D. Wallace, Program developed for CO_2 system calculations, *Rep. 105*, 33 pp., Oak Ridge Natl. Lab., Carbon Dioxide Inf. Anal. Cent., Feb. 1998, (Also available at http://cdiac.esd.ornl.gov/cdiac/oceans/co2rprt.html).

Lisitzin, A. P., *Sedimentation in the World Ocean*, *Spec. Publ. 17*, 218 pp., Soc. Econ. Paleontol. and Mineral., Am. Assoc. of Pet. Geol., Tulsa, Okla., 1972.

Mantyla, A. W., and J. L. Reid, Abyssal characteristics of the World Ocean waters, *Deep Sea Res.*, *30*, 805–833, 1983.

Mehrbach, C., C. H. Culberson, J. E. Hawley, and R. M. Pytkowicz, Measurement of the apparent dissociation constants of carbonic acid in seawater at atmospheric pressure, *Limnol. Oceanogr.*, *18*, 897–907, 1973.

Millero, F. J., The thermodynamics of seawater at one atmosphere, *Ocean Sci. Eng.*, *7*, 403–460, 1982.

Millero, F. J., Influence of pressure on chemical processes in the sea, in *Chemical Oceanography*, 2nd ed., vol. 8, edited by J. P. Riley and R. Chester, chap. 43, pp. 1–88, Academic, San Diego, Calif., 1983.

Millero, F. J., Thermodynamics of the carbon dioxide system in the oceans, *Geochim. Cosmochim. Acta*, *59*(4), 661–677, 1995.

Millero, F. J., K. Lee, and M. Roche, Distribution of alkalinity in the surface waters of the major oceans, *Mar. Chem.*, *60*, 111–130, 1998a.

Millero, F. J., et al., Total alkalinity measurements in the Indian Ocean during the WOCE Hydrographic Program CO_2 survey cruises 1994–1996, *Mar. Chem.*, *63*, 9–20, 1998b.

Milliman, J. D., P. J. Troy, W. M. Balch, A. K. Adams, Y.-H. Li, and F. T. Mackenzie, Biologically mediated dissolution of calcium carbonate above the chemical lysocline, *Deep Sea Res., Part I*, *46*, 1653–1669, 1999.

Mintrop, L., A. Kortzinger, and J. C. Duinker, The carbon dioxide system in the northwestern Indian Ocean during south-west monsoon, *Mar. Chem.*, *64*, 315–336, 1999.

Morris, A. W., and J. P. Riley, The bromide/chlorinity and sulphate/chlorinity ratio in sea water, *Deep Sea Res.*, *13*, 699–705, 1966.

Mucci, A., The solubility of calcite and aragonite in seawater at various salinities, temperatures and one atmosphere total pressure, *Am. J. Sci.*, *283*, 780–799, 1983.

Murray, J., and J. Chumley, The deep sea deposits of the Atlantic Ocean, *Trans. R. Soc. Edinburgh*, *54*, 1–252, 1924.

Poisson, A., B. Schauer, and C. Brunet, Les Rapports des campagnes a la mer, MD43/INDIGO 1, *Les publ. de la mission de recherche des Terres Australes et Antarctiques Françaises 85-06*, 267 pp., Univ. Pierre et Marie Curie, Paris, 1988.

Poisson, A., B. Schauer, and C. Brunet, Les Rapports des campagnes a la mer, MD49/INDIGO 2, *Les publications de la mission de recherche des Terres Australes et Antarctiques Françaises*, *Rep. 86-02*, 234 pp., Univ. Pierre et Marie Curie, Paris, 1989.

Poisson, A., B. Schauer, and C. Brunet, Les Rapports des campagnes a la mer, MD53/INDIGO 3, *Les publications de la mission de recherche des Terres Australes et Antarctiques Françaises*, *Rep. 87-02*, 269 pp., Univ. Pierre et Marie Curie, Paris, 1990.

Pond, D. W., R. P. Harris, and C. A. Brownlee, Microinjection technique using a pH sensitive dye to determine the gut pH of Calanus helgolandicus, *Mar. Biol.*, *123*, 75–79, 1995.

Rao, C. K., S. W. A. Naqvi, M. D. Kumar, S. J. D. Varaprasad, D. A. Jayakumar, M. D. George, and S. Y. S. Singbal, Hydrochemistry of the Bay of Bengal: Possible reasons for a different water-column cycling of carbon and nitrogen from the Arabian Sea, *Mar. Chem.*, *47*, 279–290, 1994.

Redfield, A. C., B. H. Ketchum, and F. A. Richards, The influence of organisms on the composition of sea water, in *The Sea*, vol. 2, edited by M. N. Hill, pp. 26–77, Wiley-Interscience, New York, 1963.

Riley, J. P., The occurrence of anomalously high fluoride concentrations in the North Atlantic, *Deep Sea Res.*, *12*, 219–220, 1965.

Rubin, S., and R. M. Key, Separating natural and bomb-produced radiocarbon in the ocean: The potential alkalinity method, *Global Biogeochem. Cycles*, in press, 2002.

Sabine, C. L., and F. T. Mackenzie, Bank-derived carbonate sediment transport and dissolution in the Hawaiian Archipelago, *Aquat. Geochem.*, *1*, 189–230, 1995.

Sabine, C. L., R. M. Key, K. M. Johnson, F. J. Millero, A. Poisson, J. L. Sarmiento, D. W.R. Wallace, and C. D. Winn, Anthropogenic CO_2 inventory of the Indian Ocean, *Mar. Chem.*, *13*(1), 179–198, 1999.

Sabine, C. L., R. A. Feely, R. M. Key, J. L. Bullister, F. J. Millero, K. Lee, T.-H. Peng, B. Tilbrook, T. Ono, and C. S. Wong, Distribution of anthropogenic CO_2 in the Pacific Ocean, *Global Biogeochem. Cycles*, doi:10.1029/2001GB001639, in press, 2002.

Sarma, V. V. S. S., and P. V. Narvekar, A study on inorganic carbon components in the Andaman Sea during the post monsoon season, *Oceanol. Acta*, *24*, 125–134, 2001.

Sen Gupta, R., and S. W.A. Naqvi, Chemical oceanography of the Indian Ocean, north of the equator, *Deep Sea Res.*, *31*, 671–706, 1984.

Sen Gupta, R., S. Naik, and S. Y. S. Singbal, A study of fluoride, calcium and magnesium in the northern Indian Ocean, *Mar. Chem.*, *6*, 125–141, 1978.

Sen Gupta, R., C. Moraes, M. D. George, T. W. Kureishy, R. J. Noronha, and S. P. Fondekar, Chemistry and hydrography of the Andaman Sea, *Indian J. Mar. Sci.*, *10*, 228–233, 1981.

Siegenthaler, U., and J. L. Sarmiento, Atmospheric carbon dioxide and the ocean, *Nature*, *365*, 119–125, 1993.

Sverdrup, H. U., N. W. Johnson, and R. H. Fleming, *The Oceans*, Prentice-Hall, Old Tappan, N. J., 1941.

Toole, J. M., and B. A. Warren, A hydrographic section across the subtropical South Indian Ocean, *Deep Sea Res., Part I*, *40*, 1973–2019, 1993.

Uppström, L. R., Boron/chlorinity ratio of deep-sea water from the Pacific Ocean, *Deep Sea Res.*, *21*, 161–162, 1974.

Volk, T. and M. I. Hoffert, Ocean carbon pumps: Analysis of relative

strengths and efficiencies in ocean-driven atmospheric CO_2 changes, in *The Carbon Cycle and Atmospheric CO_2: Natural Variations Archean to Present*, *Geophys. Monogr. Ser.*, vol. 32, edited by E. T. Sundquist and W. S. Broecker, pp. 99–110, AGU, Washington, D.C., 1985.

Weiss, R., Carbon dioxide in water and seawater: The solubility of a non-ideal gas, *Mar. Chem.*, *2*, 203–215, 1974.

Wessel, P., and W. H. F. Smith, New version of generic mapping tools released, *Eos Trans. AGU*, *76*, 329, 1995.

Wyrtki, K., Physical oceanography of the Indian Ocean, in *Ecological Studies: Analysis and Synthesis*, vol. 3, edited by B. Zeitzschel, pp. 18–36, Springer-Verlag, New York, 1973.

Yao, W., and F. J. Millero, The chemistry of the anoxic waters in the Framvaren Fjord, Norway, *J. Aquat. Geochem.*, *1*, 53–88, 1995.

R. A. Feely and D. Greeley, NOAA/Pacific Marine Environmental Laboratory, 7600 Sand Point Way NE, Seattle, WA 98115, USA.

R. M. Key, Atmospheric and Oceanic Sciences Program, Princeton University, Forrestal Campus/Sayre Hall, Princeton, NJ 08544, USA.

C. L. Sabine, Joint Institute for the Study of Atmosphere and Ocean, University of Washington, c/o NOAA/PMEL, 7600 Sand Point Way NE, Seattle, WA 98115, USA. (sabine@pmel.noaa.gov)